DESCRIPTION OF A THERMODYNAMIC OCEAN MODELLING SYSTEM TOMS

by Tommy G. Jensen

David A. Randall, Principal Investigator

Colorado State University

DEPARTMENT OF ATMOSPHERIC SCIENCE

PAPER NO. 670

DESCRIPTION OF A THERMODYNAMIC OCEAN MODELLING SYSTEM TOMS

by

Tommy G. Jensen

Research supported by the
U.S. Department of Energy
under Grant number DE-FG03-96ER62167

Department of Atmospheric Science
Colorado State University
Fort Collins, CO

December 1998

Atmospheric Science Paper No. 670

Abstract

A new quasi-isopycnal ocean model is presented. The model has full prognostic equations for momentum, temperature, salinity and tracers. Bottom topography can be included or the model can be used in a reduced gravity upper ocean mode. As an option, the model can be run without prognostic thermodynamics. An arbitrary Lagrangian-Eulerian (ALE) coordinate is used in the vertical, making the model a hybrid between a traditional z–coordinate model and an isopycnal model. In the horizontal, spherical ccordinates or rectangular coordinates may be used. The mixed layer formulation is of Kraus-Turner type with added entrainment due to shear. Vertical diffusion of momentum, heat, salt and other tracers is incorporated using a Richardson number dependent formulation. Horizontal diffusion can be any combination of harmonic and biharmonic friction. The coastlines can be irregular and have open boundaries. Many open boundary conditions are available. Test results for oceanic upwelling regimes are given.

Chapter 1

Introduction

Ocean modelling has received more attention in recent years, but is still lacking the level of sophistication found in atmospheric models. Considering the dominant role the ocean plays in controlling our climate, an increased effort is needed to bring our ocean modelling capability up to date and improve the realism of coupled ocean-atmosphere models.

A major obstracle for realisticly modelling the ocean to date has been lack of computer resources. The internal radius of deformation, which determines the horizontal resolution needed for modelling instabilities, eddies and fronts in geophysical flows, is typically 10-50 km for the ocean compared to 1000 km for the atmosphere. Global or basin scale ocean models that adequately resolve this small scale have not been run yet. With massively parallel computers, however, such eddy-resolving oceanic general circulation models will be possible in the near future. The CHAMMP research initiative has given ocean modellers an opportunity to prepare for the hardware and availability of high resolution models.

The advantages of using potential density as a vertical coordinate are well documented (e.g. Bleck and Boudra, 1986, Hsu and Arakawa, 1990), while the disadvantage has been associated vanishing layers. Arakawa and Hsu, (1990) have recently devised new numerical schemes which partly eliminate this problem. The model developed here is based on the philosophy that isopycnal models have the desired feature, that motion takes place along isopycnal surfaces. However, the constraints imposed on the

exchange of fluid between isopycnal layers lead to new technical difficulties. Although practical methods exist to deal with these, e.g. Bleck et al., (1989), Oberhuber, (1993), the approach here has been to relax the requirements of isopycnal coordinates. However, in most cases, the density variation in a layer is small compared to the variation between layers at a given geographical location, so the model locally will behave more like an isopycnal model than a z-coordinate model. Transfer of fluid between layers can be controlled and no numerical vertical diffusion exists in the model. This numerical strategy of changing from a Lagrangian to an Eulerian approach was developed at Los Alamos (Hirt et al., 1974) and is referred to as the Arbitrary Lagrangian-Eulerian (ALE) method. A review of these methods can be found in Benson (1992).

In this report a new Thermodynamic Ocean Modelling System (TOMS) is described in detail. TOMS is based on the ALE vertical coordinate and is as a result a hybrid between isopycnal and z-coordinate models. The modelling system is designed for oceanic and coastal flows where the aspect ratio is small. It is based on the hydrodynamic multi-layer reduced gravity model by Jensen (1991, 1993), but now also includes prognostic temperature, salinity and tracers as well as mixed layer physics. In addition to being an upper ocean model, it can be configured with finite depth, including bottom topography in the lowest layer. In addition, a simple data assimilation scheme, and a number of new open boundary conditions, which increase the range of possible applications of TOMS, have been included.

Mixed layer physics has been fully incorporated in the model as proposed. The two uppermost layers have implemented Kraus-Turner mixed layer physics, extended to include exponential damping of TKE, and convective overturning. Inclusion of shear induced mixing at the base of all dynamic layers is represented by a Richardson number dependent mixing. An entrainment and detrainment formulation is used in conjunction with a diffusion coefficient formulation. This mixed layer scheme is different than those used in isopycnal models.

Chapter 2

Ocean Model

The ocean model is based on the hydrodynamical multi-layer model by Jensen (1991; 1993), modified to include bottom topography (Jensen, 1996) and prognostic scalar variables such as temperature and salinity. Layer depths may also vary in time and space. For many transient phenomena, such as a internal wave, the layers remain material layers. However, in situations where upwelling or downwelling takes place over a long period, exchange of fluids takes place between the layers. For this reason, the uppermost layers are allowed to have variable densities. This in particular allows a realistic ocean mixed layer. Figure 2.1 shows the model structure in the vertical: At the upper ocean are a number of variable density layers to simulate air-sea interactions. Below, a number of intermediate depth layers may be kept isopycnal above an abyss of finite or infinite depth. When the latter approximation is made, the fast barotropic mode is removed.

The model equations are given in spherical coordinates, so they also apply for length scales larger than the oceanic barotropic deformation radius. Consider an ocean consisting of N layers of uniform density as shown in Fig. 2.1. The layers are labelled with increasing numbers downward. Let us assume that all layers have a positive thickness everywhere. This implies that layers are not allowed to surface or merge, and that the bottom topography is always in the lowest layer.

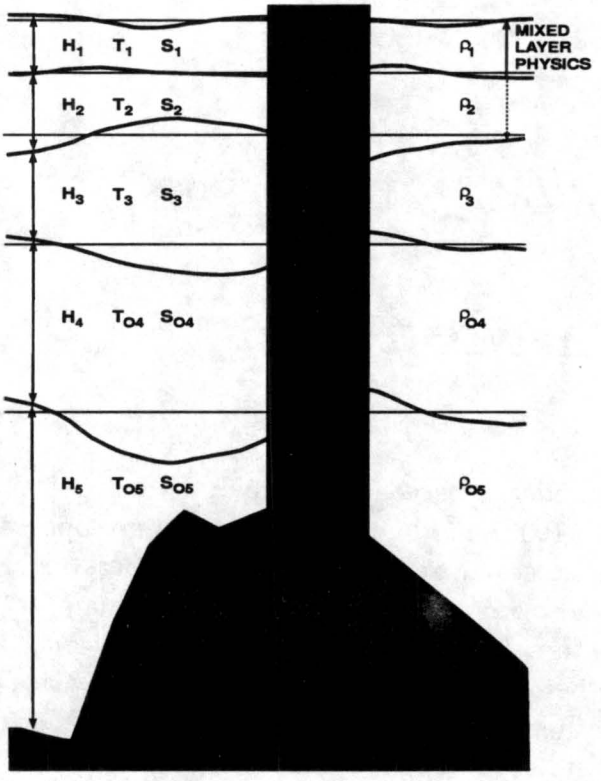

Figure 2.1: Vertical model structure with bottom topography confined to the deepest layer.

2.1 Momentum Equations in Transport Form

Let the velocity components toward the east and north be u and v, respectively. We choose $z = 0$ to be the surface of the ocean at rest. Define vertically integrated volume transport components U_j and V_j by

$$U_j = \int_{z_j}^{z_{j+1}} u \, dz \tag{1}$$

between two isopycnal surfaces $z_j(x, y, t)$ and $z_{j+1}(x, y, t)$, with an equivalent expression for V_j. The thickness of layer j defined by this integration, is $H_j = (z_{j+1} - z_j)$ and the vertically averaged density is ρ_j. The transport equation for U_j becomes

$$\frac{\partial U_j}{\partial t} + \frac{1}{a\cos\theta}\frac{\partial}{\partial\phi}\left(\frac{U_j^2}{H_j}\right) + \frac{1}{a}\frac{\partial}{\partial\theta}\left(\frac{U_j V_j}{H_j}\right) - \frac{2U_j V_j \tan\theta}{aH_j} - fV_j$$

$$= \frac{-H_j}{\rho_j a\cos\theta}\frac{\partial P_j}{\partial\phi} + \frac{w_{ej}U_{j+1}/H_{j+1} - w_{e(j-1)}U_j/H_j}{H_j} + \mathcal{T}_j^{\phi} \tag{2}$$

Similarly for V_j, we have

$$\frac{\partial V_j}{\partial t} + \frac{1}{a\cos\theta}\frac{\partial}{\partial\phi}\left(\frac{U_j V_j}{H_j}\right) + \frac{1}{a}\frac{\partial}{\partial\theta}\left(\frac{V_j^2}{H_j}\right) + \frac{(U_j^2 - V_j^2)\tan\theta}{aH_j} + fU_j$$

$$= \frac{-H_j}{\rho_j a}\frac{\partial P_j}{\partial\theta} + \frac{w_{ej}V_{j+1}/H_{j+1} - w_{e(j-1)}V_j/H_j}{H_j} + \mathcal{T}_j^{\theta} \tag{3}$$

Here g is the acceleration of gravity, $f = 2\Omega sin(\theta)$ is the Coriolis parameter where Ω is the rate of rotation of the Earth, and $\mathcal{T}_j$ represents turbulent stresses in each layer, where the superscripts denote the ϕ or θ component.

In (2) and (3) the vertically integrated pressure gradient is given by

$$\nabla P_j = g\left(\gamma\rho_j\nabla\eta + \frac{H_j}{2}\nabla\rho_j - \sum_{i=1}^{j-1}[(\rho_j - \rho_i)\nabla H_i - H_i\nabla\rho_i]\right) \tag{4}$$

where the second term ensures that the current in the layer is depth independent (McCreary and Kundu, 1988). The factor γ can be chosen to

be less than 1 in order to slow down the phase speed for the barotropic gravity waves with little influence on the baroclinic modes (Jensen, 1996). With N layers the surface displacement η is given by

$$\eta = \sum_{i=1}^{N}(H_i - H_{0i}), \tag{5}$$

and H_{0j} is the thickness of layer j at rest.

The model allow several choices of parameterizations of turbulent momentum fluxes. In order to include classical representations for horizontal and vertical directions, we write for the zonal direction

$$\mathcal{T}_j^{\phi} = \mathcal{F}_j^{\phi} + \frac{\tau_j^{\phi,t}}{\rho_j} - \frac{\tau_j^{\phi,b}}{\rho_j} + \mathcal{D}_j^{\phi} \tag{6}$$

with a similar expression for the meridional direction. In (6), $\mathcal{F}$ represents the eddy stresses due to unresolved horizontal scales of motion, and τ is the tangential stress due to vertical friction and the superscripts denote the ϕ or θ component and top or bottom of the layer, while $\mathcal{D}_j^{\phi}$ is due to internal stresses within each layer. The exact form of these stresses depends on the parameterization, but most often a form in analogy to anisotropic molecular viscosity is assumed. For nondivergent horizontal velocities the following form is used:

$$\mathcal{F}_j^{\phi} = A_j H_j \left[\nabla^2(\frac{U_j}{H_j}) - \frac{1}{a^2\cos^2\theta}\left[\frac{U_j}{H_j}(1-2\cos^2\theta) + 2\sin\theta\,\frac{\partial}{\partial\phi}(\frac{V_j}{H_j})\right]\right]$$

$$-A_{4,j}H_j\nabla^4(\frac{U_j}{H_j}) - A_n\frac{\Delta t}{2}\left[(\frac{U_j}{H_j})^2\frac{1}{a^2\cos^2\theta}\frac{\partial^2 U_j}{\partial\phi^2} + (\frac{V_j}{H_j})^2\frac{1}{a^2}\frac{\partial^2 U_j}{\partial\theta^2}\right] \tag{7}$$

and

$$\mathcal{F}_j^{\theta} = A_j H_j \left[\nabla^2(\frac{V_j}{H_j}) - \frac{1}{a^2\cos^2\theta}\left[\frac{V_j}{H_j}(1-2\cos^2\theta) - 2\sin\theta\,\frac{\partial}{\partial\phi}(\frac{U_j}{H_j})\right]\right]$$

$$-A_{4,j}H_j\nabla^4(\frac{V_j}{H_j}) - A_n\frac{\Delta t}{2}\left[(\frac{U_j}{H_j})^2\frac{1}{a^2\cos^2\theta}\frac{\partial^2 V_j}{\partial\phi^2} + (\frac{V_j}{H_j})^2\frac{1}{a^2}\frac{\partial^2 V_j}{\partial\theta^2}\right] \tag{8}$$

Here A_j is an eddy viscosity, which is allowed to vary in space. The form of the differential harmonic operator on the velocity is that given by Semtner (1986). The biharmonic friction coefficient $A_{4,j}$ is constant for each layer, and the non-linear, velocity dependent eddy viscosity with a non-dimensional amplitude A_n, is given by Abbott et al., 1981. These terms are part of the third order correction terms to the central, second order finite difference approximation of the non-linear terms in the momentum equation. However, since the net effect is to selectively diffuse high velocity shear, we find it appropiate to include them explicitly as an additional eddy viscosity. In order for the terms to have the same magnitude as in the Taylor expansion for the non-linear terms, $A_n = 1$ should be selected. Along coastal boundaries the vorticity transfer is controlled using a free slip, partial slip, no slip or hyper frictional boundary condition (Jensen, 1994). The vertical stress for the x-direction at the top of each layer is

$$\tau_j^{\phi,t} = \tau_w^{\phi}\delta_{1j} + \rho_j A_z\Big(\frac{U_{j-1}}{H_{j-1}} - \frac{U_j}{H_j}\Big)\frac{2}{H_{j-1}+H_j}(1-\delta_{1j}) \tag{9}$$

and at the bottom

$$\tau_j^{\phi,b} = \rho_j A_z\Big(\frac{U_j}{H_j} - \frac{U_{j+1}}{H_{j+1}}\Big)\frac{2}{H_j+H_{j+1}}(1-\delta_{Nj}) \tag{10}$$

with equivalent expressions for the meridional direction. In these expressions, τ_w denotes a wind stress, δ_{ij} is the Kronecker delta, A_z is the vertical diffusivity, and R is a bottom friction coefficient.

The term $\mathcal{D}_j$ represents other, small scale turbulent stress parameterizations. We have included the following terms, only shown for the zonal direction:

$$\mathcal{D}_j^{\phi} = -R_j^U U_j - \frac{c_\tau}{H_j}\Big(\frac{U_j}{H_j}\Big)^3 \tag{11}$$

where the Newtonian coefficient R_j can be different for the U and V component and vary in space. This is practical for parameterization of small scale topography as discussed later. The second term in (11) dissipates strong flow in thin layers, which is a simple parameterization for transition to turbulence within a layer.

Finally, the wind stress components are computed from

$$\tau_w^{\phi} = \rho_a c_d((U_a - U_1/H_1)^2 + (V_a - V_1/H_1)^2)^{1/2}(U_a - U_1/H_1) \qquad (12)$$

and

$$\tau_w^{\theta} = \rho_a c_d((U_a - U_1/H_1)^2 + (V_a - V_1/H_1)^2)^{1/2}(V_a - V_1/H_1) \qquad (13)$$

where ρ_a is the density of air, U_a and V_a is the zonal and meridional wind velocity component, and c_d is a constant drag coefficient. Note that the stress is based on the differential velocity between the ocean and the wind rather than the wind velocity alone.

2.2 Continuity Equation

The continuity equation becomes

$$\frac{\partial H_j}{\partial t} + \frac{1}{a\cos\theta}\left[\frac{\partial U_j}{\partial \phi} + \frac{\partial}{\partial \theta}(V_j \cos\theta)\right] = w_{ej} - w_{e(j-1)} + A_H \nabla^2 H_j + (P - E)\delta_{j1} \qquad (14)$$

where A_H is an eddy diffusion coefficient and $(P - E)$ is a source/sink due to net precipitation/evaporation. The w_e vertical velocity terms are due to entrainment by shear instability and entrainment/detrainment by buoyancy forcing and wind forcing, e.g.

$$w_{ej} = \delta_{j1} w_k + w_{sj} + w_{dj} + w_{nj} = w_{pj} + w_{nj} \qquad (15)$$

where the first term is only active for the top layer. A term due to interfacial stress, w_{sj} is positive for a layer in case its thickness becomes less that a minimum depth $H_{\min,j}$, either a preset value or determined by a bulk Richardson number, (McCreary and Kundu, 1988, 1989). This entrainment due to shear helps prevent the interface between the first two layers from surfacing; it is usually zero for deeper layers. The shear entrainment velocity is calculated as

$$w_{sj} = \frac{(H_j - H_{\min,j})^2}{\tau_e H_{\min,j}} \Theta(H_{\min,j} - H_j)\ , \qquad (16)$$

where Θ is the unit step function, which has the value 1 for positive arguments and zero otherwise. The depth, $H_{\mathrm{min},j}$, where entrainment becomes active can be selected as a constant depth or given by

$$H_{\mathrm{min},j} = H_j \, \mathrm{Ri_c}/\mathrm{Ri}. \tag{17}$$

The Richardson number, Ri, is calculated using finite differences in the vertical. In that case, eq. (16) is equivalent to

$$w_{sj} = H_j \frac{(\mathrm{Ri_c} - \mathrm{Ri})^2}{\tau_e \mathrm{Ri_c} \mathrm{Ri}} \Theta(\mathrm{Ri_c} - \mathrm{Ri}) \, , \tag{18}$$

where $\mathrm{Ri_c}$ is a preset critical Richardson number.

Where constant convergence occurs, the layer thickness may become rather large after a while. In the real ocean, sinking water is subducted when the heat flux into the ocean is positive. In order to limit the layer thickness, a detrainment velocity is defined as

$$w_{dj} = -\Theta(B) \frac{(H_j - H_{\mathrm{max},j})^2}{\tau_d H_{\mathrm{max},j}} \Theta(H_j - H_{\mathrm{max},j}) \, , \tag{19}$$

where τ_d is a time scale over which the detrainment takes place and B the buoyancy flux defined below.

The terms discussed sofar are based on mixed layer physics and are their sum denoted w_{pj}. In addition, a numerical vertical velocity w_{nj} due to coordinate motion may be present as discussed later.

2.3 Mixed Layer Model

The uppermost layer is subject to Kraus-Turner mixing. The net production of turbulent kinetic energy (TKE), q, is given by

$$q = g_1 u_*^3 - (g_2 B + g_3 \varepsilon) \, H_1 \tag{20}$$

where the friction velocity, u_*, is

$$u_* = \sqrt{\tau_1^t / \rho_1} \tag{21}$$

the buoyancy flux is B, the rate of dissipation of TKE is ε, and ρ_a is the density of air. Each term is multiplied by a factor g_1, g_2 or g_3, respectively, as discussed below. The bouyancy flux, B, is calculated as

$$B = \frac{g}{\rho_1}(\alpha Q/c_w + g\beta(E-P)S) \tag{22}$$

where $\alpha = \rho^{-1}(\partial\rho/\partial T)$ is the thermal expansion coefficient for sea water, Q the upward heat flux, c_w the specific heat of sea water, β the haline expansion coefficient, defined in the same way as β, E and P are the evaporation and precipitation respectively, and S is the salinity in practical salinity units (psu).

Different bulk formulation can be chosen by specifying the g_i factors in (20). The formulation in TOMS follow that of Oberhuber (1993). Here the efficiency factor for wind generated turbulence is

$$g_1 = 2m_0 \exp(-\frac{H_1 f}{\kappa u_*}), \tag{23}$$

with $m_0 = 1.2$, $\kappa = 0.4$ and f is the Coriolis parameter. For buoyancy driven turbulence

$$g_2 = \exp(-\frac{H_1 f}{\mu u_*}). \tag{24}$$

where

$$\mu = 2.0\Theta(B) + \kappa(1 - \Theta(B)) \tag{25}$$

where Θ is the Heaviside step function defined previously. Since dissipation is already taken into account in (23) and (24), the term in (20) is set to zero, i.e.

$$g_3 = 0. \tag{26}$$

For negative production of TKE ($q < 0$), e.g. the mixed layer is warming up or become less salty due to net precipitation, we have detrainment towards a new equilibrium depth, h_m:

$$h_m = \xi_{MO}\ \max(\min(g_1 u_*^3/(g_2 B + g_3\varepsilon)\ , H_1)\ , h_{\min}) + (1 - \xi_{MO})H_1 \tag{23}$$

which in this case is the Monin-Obukov depth. In order to keep a finite upper layer depth, a minimum depth, $h_{\min}$, can be specified. Note that

the minimum function ensures that negative production of TKE cannot deepen the mixed layer. The factor ξ_{MO}, in the range $0-1$ is introduced to approach h_m over a finite time rather than instantaneously. A value of ξ_{MO} =0.1 is used.

When we have a positive production of TKE,($q \geq 0$), either due to cooling, evaporation or wind stirring, the mixed layer entrains towards:

$$h_m = \min(H_1 + 2\rho_1 q \Delta t/(g(\rho_2 - \rho_1)H_1),\ H_{\max}) \tag{24}$$

where H_{turbl} is a penetration depth scale for the surface generated TKE. The resulting detrainment/entrainment velocity (buoyancy and wind)

$$w_k = (h_m - H_1)/(2\Delta t) \tag{25}$$

2.4 Arbitrary Langrangian Eulerian coordinate control

Very thin layers or even negative layer thickness presents a numerical problem. The ALE method consists of two main steps: A Lagrangian timestep that moves the interface without any mass crossing it, followed by a remap step that repositions the interface and computes the associated mass flux across it. In TOMS it has been implemented as described below.

The term w_{nj} in (15) becomes non-zero if a layer thickness is outside numerical preset limits. In that case, excess divergence or convergence is computed as a entrainment or detrainment rate across the base of the layer and the interface is positioned at the the level determined by this numerical limitation. As long as the divergence violates the preset criteria, the layer thickness is held fixed. However, the layer is usually not be fixed in the vertical, since other layers most likely will change their thickness. The formulation for the movement of coordinates is as follows: First step increase the entrainment of a thin layer to be as strong as the layer above, i. e.

$$w_{n1j} = \Theta(w_{p(j-1)})(\max(w_{p(j-1)}, w_{pj}) - w_{pj})\Theta(H_{\min,j} - H_j) \tag{25}$$

Next step limits the detrainment to half the layer thickness or the entrainment to half the layer thickness below, i. e.

$$w_{n2j} = (1 - \Theta(w_{n1j}) \max(w_{n1j}, -H_j/(2dt)) + \Theta(w_{n1j} \min(w_{n1j}, H_{j+1}/(2dt)) \tag{25}$$

Finally, a the divergence and convergence is limited as follows in the continuity equation.

$$w_{nj} = \Theta(D_{\min} - H_j)$$

2.5 Vertical Diffusion

Vertical mixing is added to the model in addition to the mixing described above. The vertical flux of a quantity Ψ is given by

$$F_\Psi = (A_\Psi \frac{\partial \Psi}{\partial z})^{t,b} \tag{26}$$

and evaluated at the top, (t), or bottom, (b), of each layer. The exchange coefficients, A_Ψ can be constants or evaluated after the formulation by Pacanowski and Philander (1981). In that case the coefficients depend on the Richardson number, Ri:

$$A_\Psi = \frac{A_{\Psi o}}{(1 + \alpha R_i)^n} + A_{\Psi b}. \tag{27}$$

where $A_{\Psi b}$ is a constant background diffusivity. For momentum, Pacanowski and Philander (1981) also used a constant value for $A_{\Psi o} = A_{V o}$ and $n = 2$, while temperature and salinity used $A_{\Psi o} = A_V$, e.g. the turbulent diffusion of momentum and $n = 1$. They used $\alpha = 5$.

2.6 Tracers

For tracers, for instance potential temperature T and salinity S, the conservation equation is of form

$$\frac{D\Psi_j}{Dt} = K_\Psi \nabla^2 \Psi_j + \frac{Q_\Psi}{H_j} \delta_{1j} - w_{ej}(\Psi_j - \Psi_{j+1})/H_j + Q_{c\Psi j} \tag{28}$$

where Ψ is any tracer. The term Q_Ψ is the net surface tracer flux, Q_c is exchange due to convection, and δ is the Kronecker delta. In addition to temperature and salinity, the model allows for any number of additional tracers. In particular, passive tracers can be used to follow water masses or, if source and sink terms are provided, to model chemical tracers such as oxygen, nitrate and phosphate.

2.7 Equation of State

Density is computed from potential temperature and salinity. However, since TOMS primarily is an upper ocean model, the currently used equation of state does not destinction between in situ temperature and potential temperature. Two equations of state as use. The simplest is linear in temperature and salinity. A more accurate version is a second order polynomial version given by Mamyev (1975).

2.8 Reduced Gravity Formulation

The barotropic pressure gradient is contained in the term where the surface deviation η appears. Because of the large phase speeds of barotropic gravity waves most numerical models have a special treatment of this mode. For instance, many authors filter out these waves by applying the rigid lid approximation, for example as in Bryan's (1969) world ocean model, or use a semi-implicit numerical scheme (O'Brien and Hurlburt, 1972, Hurlburt, 1974, Hurlburt and Thompson, 1976).

In this model an option to use the method of reduced gravity has been included., It is often applied in geophysical fluid dynamics, to remove the barotropic modes, including the planetary waves. By assuming that the pressure gradient vanishes in the lowest layer, the velocity becomes zero in the deep ocean. For consistency, it must also be assumed that the horizontal density gradients vanish in that layer. By taking the limit $H_N \rightarrow \infty$, the velocity in the bottom layer $\vec{v}_N \rightarrow 0$, and from (2) to (3) we find

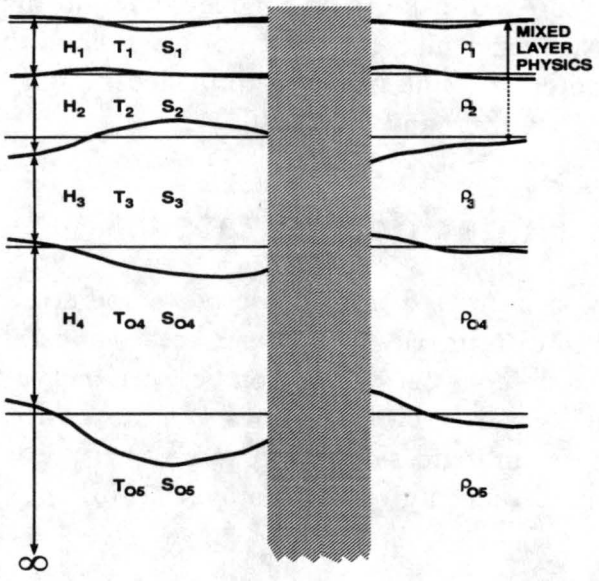

Figure 2.2: Vertical model structure for a multi-layer reduced gravity model.

that the gradient of the surface elevation is given by

$$\rho_N \nabla \eta = \sum_{i=1}^{N-1} \Big((\rho_N - \rho_i) \nabla H_i - H_i \nabla \rho_i \Big) \tag{29}$$

Since we assumed a constant $\rho_N = \rho_{No}$,

$$\rho_{No} \nabla \eta = \sum_{i=1}^{N-1} \nabla \Big((\rho_{No} - \rho_i) H_i \Big) \tag{30}$$

Figure 2.2 shows the vertical structure of a reduced gravity model. Where inclusion of bottom topography is needed, all modes must be calculated explicitly, for instance with retardation of the barotropic mode as discussed earlier ($\gamma << 1$ in eqn. 4).

Chapter 3

Open Boundary Conditions

In most applications of numerical ocean models, artificial boundaries are introduced to limit the domain. Along such a boundary we need to apply what is often referred to as an Open Boundary Condition (OBC). A number of local methods used in ocean models are implemented. They are the simple conditions: clamped, prescribed, zero gradient; radiation conditions: Camerlengo-O'Brien, Orlanski; a sponge type condition: Flow Relaxation Scheme and a method based on characteristics of the linear equations. These OBC and examples of their use in a number of idealized test cases can be found in Jensen (1998b).

3.1 Simple conditions

The simplest conditions prescribe a value of a variable or the gradient of a variable on the boundary. If one can prescribe the exact condition on the boundary consistent with the interior numerical solution, there is not an open boundary problem to be solved. In most cases only part of the solution is known, and a condition for the unknown part of the solution must be given. One possible condition is that the solution does not change in time

$$\frac{\partial \Phi}{\partial t} = 0. \tag{31}$$

which is the commonly used clamped condition.

Nearly as simple is the zero gradient condition,

$$\frac{\partial \Phi}{\partial n} = 0. \tag{32}$$

where the derivative is taken formal to the open boundary. For incident waves both these conditions are reflective. If for instance Φ equals the pressure or related variable such as a surface elevation or interface displacement, the latter condition give the same reflection as a wall condition, e.g. $u = 0$, where u is the velocity component normal to the boundary. The reflected wave using the clamped condition has opposite phase of the wave reflected from a wall. This leads to an improved condition

$$\frac{\partial \Phi}{\partial t} + \frac{\partial \Phi}{\partial n} = 0. \tag{33}$$

3.2 Radiation conditions

This class of conditions assume a free wave propagating at normal incidence on the boundary and is based on the 1-D wave equation,

$$\frac{\partial \Phi}{\partial t} + c_\Phi \frac{\partial \Phi}{\partial x} = 0. \tag{34}$$

where Φ is a field variable for which an obc is imposed. Orlanski (1976) proposed to calculate the phase speed using finite differences. If the open boundary is to the east, and the boundary at B, a non-dimensional phase speed is computed as

$$c_\Phi = \max\{-\min\{\frac{\Phi^n_{B-1} - \Phi^{n-1}_{B-1}}{\Phi^{n-1}_{B-1} - \Phi^{n-1}_{B-2}}, 1\}, 0\}. \tag{35}$$

which can be put dimensional form by multiplying by $\Delta x/\Delta t$. Note that negative values (e.g. propagation away from the boundary) of c_Φ are truncated. The boundary value using the Orlanski condition is calculated as

$$\Phi^{n+1}_B = c_\Phi \; \Phi^n_{B-1} + (1 - c_\Phi) \; \Phi^n_B. \tag{36}$$

Camerlengo and O'Brien [1980], simplified this condition by using $c_\Phi = 1$ if $c_\Phi \leq 0$, e.g. only the sign of c_Φ is used. This condition deliberately overestimates the outward propagation speed. An even simpler approach is to choose extrapolation in all cases, e.g. $c_\Phi = 1$.

The evaluation of c_Φ is simple for flows without stratification. For a layered model, a computation layer by layer is a straight forward extention of the 2-D case. This strategy will work if a single vertical mode dominates the flow. If two or more vertical modes contribute significantly to the flow simultaneously, a decomposition onto linear vertical modes are, at least in principle, a better method. For this reason, we have applied the OI and CO conditions to the amplitudes of the each vertical mode, and after computation of the boundary amplitudes, transformed back to layer formulation. This method is described in Jensen, (1993).

3.3 Characteristic conditions

By considering the system of equations as hyperbolic, the method of characteristics may be applied. If we project the equations onto linear vertical modes, we simply get a shallow water equation for each vertical mode (e.g. Gill, 1982, p. 167-175). Using the Hedstrom (1979) condition as tested by Røed and Cooper, 1987, we have

$$\frac{\partial \tilde{U}}{\partial t} = 1/2c^{(k)} \frac{\partial}{\partial x}(U - c^{(k)}\tilde{\eta}) + U_F \tag{37}$$

where $\tilde{}$ indicates a projection on linear vertical modes, $c^{(k)}$ is the phase speed of mode k, and U_F is the sum of the Coriolis term and the frictional terms.

3.4 Flow Relaxation Scheme

The strategy is to use the FRS as a frame work in which any open boundary condition may be added. Since the FRS was developed to impose boundary conditions from a large scale atmospheric model to a fine grid limited area

atmospheric model, it is practical to implement a simple data assimilation scheme (nudging) for the entire model domain. In that respect, prescribing an obc can be considered a special case of a data assimilation process. The FRS allows specification of the boundary solution for any variable as a sum of an external value and a value calculatied from the interior, i. e. an obc. The scheme is applied as follows: For any variable the interior solution $\hat{U}$ is calculated. An obc solution U_L is calculated on the open boundary from interior values. The externally imposed solution on the boundary is U_{obs}, where the subscript implies that this value often have been obtained from observations. The boundary solution is then given by

$$\tilde{\Phi} = \Phi_L + \Phi_{obs}. \tag{38}$$

The FRS technique is now applied as nudging in the vicinity of the open boundary:

$$\Phi = \alpha(x,y,z)\tilde{\Phi} + (1-\alpha(x,y,z))\hat{\Phi}, \tag{39}$$

where Φ is the updated solution, which has been relaxed towards the boundary value $\tilde{\Phi}$. The relaxation function α is usually chosen to be 1 on the boundary and decreases to zero in the interior of the domain.

The optimal width of the relaxation zone and the functional variation within it, depends on the problem. Assume that the relaxation zone extends from $x = 0$ to $x = 1$, with the boundary at $x = 1$. Martinsen and Engedahl, (1987) used widths of 3-10 grid points and used the following functions:

$$\alpha(x) = 1 - \tanh(\frac{n}{2}(1-x)) \tag{40}$$

and

$$\alpha(x) = x^2, \tag{41}$$

where n is the number of grid points in the relaxation zone. In a general purpose code, a more convenient form is

$$\alpha(x) = ((1-q)x + q)^p. \tag{42}$$

The tanh formulation provides a steeper filter function than a second order polynomial. A similar variation can be obtained using $p = 6$ and $q = 0$ in the polynomial form (42).

In the Danish Hydraulic Institute Boussinesq wave model (MIKE21BW) the expression used for sponge layers is

$$\alpha(x) = (1 - a^{b^{(1-x)^n}})\, c \tag{43}$$

with $c = 1$. This form does not equal one for $x = 1$. A polynomial with $p = 8$ and $q = 0.4$ has similar variation in the interval [0.-0.8] but goes to one for $x = 1$. Another possibility is to choose $c = a/(a-1)$ in (43). Figure 2 shows the variation over the relaxation zone for a few choices of α.

Applying the FRS technique is equivalent to changing the equations in the FRS zone. For a variable Φ, we can be write

$$\frac{\partial \Phi}{\partial t} = f(\Phi) - \frac{\alpha}{\Delta t(1-\alpha)}(\Phi - \tilde{\Phi}) \tag{44}$$

where the second term on the RHS is due to the FRS scheme. Note that this corresponds to adding a linear source/or sink term. However, the relaxation coefficient goes to infinity in the edge of the domain, where the calculated solution is replaced by the boundary solution. A finite relaxation factor is obtained using $\alpha < 1$, which corresponds to a larger time constant in the adjustment. One advantage of the form (44) is that it can be used directly in an implicit scheme.

Chapter 4

Numerical Scheme

Most terms in the model are computed using explicit schemes. This ensures very easy implementation on parallel machines. For the momentum equations, the time integration scheme is leap-frog.

A forward in time scheme is used for lateral and vertical diffusion and eddy viscosity. For Rayleigh friction terms, an implicit backward scheme can be used instead of the forward scheme for stability.

For the continuity equation and the tracer equations the model has the option of several schemes. One is the same as for the momentum equations. However, the dispersion errors, in particular in the vicinity of fronts, can be severe and negative values may occur. For this reason the positive definite scheme of Hsu and Arakawa, (1990) was also implemented. However, the computational costs are much higher than using leap-frog combined with the ALE technique. Being components or special cases of the Hsu-Arakawa scheme, the first-order upstream difference (or donor cell), the Lax-Wendroff scheme, Fromm's scheme and the Takacs scheme is also available. Finally, a third order upstream differencing scheme (Leonard, 197) has been implemented for tracer advection.

For discretization in space the C-grid is used (Arakawa and Lamb, 1977). This implies second order accuracy except for the lateral eddy diffusivity terms which are only first order. The grid spacing is assumed constant, but may be different for zonal and meridional directions. The coordinate system is spherical or rectangular. In the latter case the model

has the option of a β-plane, f-plane approximation or no rotation. These features make it more convenient to compare the numerical model results against analytical solutions.

In order to filter out time computational mode associated with the leap-frog scheme a forward scheme can be applied after a number of leap-frog steps (Lilly, 1965). Typically every 99 steps are forward steps. Alternatively, a time filter (Asselin, 1972) may be applied. Let χ be any of the variables, U, V and H. Then

$$\chi_1^n = \chi^n + \frac{1}{2}\nu(\chi_1^{n-1} - 2\chi^n + \chi^{n+1}) \tag{45}$$

where ν, the filter factor is suggested to be in the range 0.1 - 0.8 according to James, (1987). Finally, a time avering between two time steps is also implemented as a filter.

Chapter 5

Applications

A particular difficult problem for layered isopycnal models is to model a steady state upwelling or downwelling regime. The layer may tend to vanish or become unrealisticly deep. The entrainment and detrainment parameterization adopted above may be used to prevent this. As examples the zonal and meridional overturning in the equatorial current system and coastal upwelling regimes in the tropics are used to test the model. The main reasons for choosing this system is the fast equatorial response so that the model can be spun up from rest, and that the large radius of deformation allow us to use coarser resolution. Also a small equatorial ocean is used: 20°wide and spans from 10°S to 10°N. Only two layers are active over an infinitely deep third layer, i.e. a 2.5 layer model is used. The thickness of the upper layer (layer 1) is initially 75 m and the intermediate layer (layer 2) is initially 325 m thick. The temperatures for the three layers are 20°C, 5°C, and 0°C, while the salinities are 32 psu, 34 psu and 35 psu respectively.

The table below gives the parameters used in the box models in this section.

Table 1. Parameters used in Box model runs.

Parameter:	Value:	Unit	Case
time step	1800	sec	1-6
Δ x, Δ y	1/2°		1-6
$H_{1,0}$, $H_{2,0}$	75, 325	m	1-6
T_1, T_2, T_3	20., 5., 0.	°C	3-6
S_1, S_2, S_3	32., 34., 35.	°C	4-6
harmonic viscosity, diffusivity	1000., 600.	m^2/s	1-6
bi-harmonic viscosity	10^{10}	m^4/s	1-6

The runs discussed below are forced by a spatial uniform wind stress which is applied to an ocean initially at rest. A linear increase from no wind to a steady wind forcing is done over 10 days to limit the generation of high-frequency internal waves. The models were integrated for 30 days. Since the domain is closed, coastal Kelvin waves propagate along the boundaries and will influence the solution along the western boundary for longer integrations.

5.1 Westward Equatorial Jet

On the equator, strong easterly winds will create an intense westward oceanic jet, while the response off the equator will produce a poleward surface flow and consequently equatorial upwelling. This is is the traditional equatorial upwelling regime as observed in the Pacific Ocean. Upwelling, and consequently the mixed layer physics, is clearly an important factor in maintaining the relatively low SST in the area. However, current are also strong, so non-linear effects may also be of importance. The following cases demonstrates that this is in fact the case for TOMS.

Six different runs were made: a linear case where the wind stress was limited to half the magnitude used in subsequent runs (case 1), a linear case with active fluid exchange between layers (case 2), a non-linear case, i.e. adding momentum advection (case 3), a non-linear run with prognostic temperature (case 4), a non-linear run with fully prognostic temperature and salinity (case 5), and finally a case with prognostic temperature and salinity, but without advection of momentum (case 6).

In cases (1-4) the salinity is kept constant. For case 1-3 the temperature is also kept constant. Cases 2 and 3 were made to assess the importance of entrainment and momentum advection, respectively. When the wind forcing is weak, entrainment or detrainment does not take place and non-linear advection is not important. In the runs (cases 1 and 2) presented here, momentum advection is actually turned off, to be sure that the results are truly linear. The linear test runs are made to compare the model to analytical calculations, i. e. Yoshida (1959).

Figure 5.1 shows the result of a linear run, where only hydrodynamic effects are active. The wind stress were limited to 0.03 N/m^2 in order to prevent surfacing of the isopycnals and entrainment of fluid from layer 2 into layer 1. The upper layer becomes initially shallow along the equator until advection build up a thick upper layer along the eastern wall. Since no mass exchange takes place between layer 1 and layer 2, each layer have two closed gyres, one in each hemisphere, which are established after about 1 month of spin up. The most dominant feature is the equatorial undercurrent driven by the east-west pressure gradient along the equator. Maximum current in the upper layer is 0.87 m/s and 0.087 m/s in layer 2.

What happens if we add more physics? Figure 5.2 shows the result from a run with active entrainment added (case 2). The intensity of the upwelling increases with the wind stress and in order to enhance the differences from the purely linear run, the wind stress was increased by a factor of 2, to 0.06 N/m^2. We note several differences: The equatorial jet has become divergent at the surface and the undercurrent is convergent. These effects are entirely due to entrainment of water from layer 2 into layer 1. Note that adding mixed layer physics and consequently entrainment reduces the negative thickness anomaly on the equator compared to case 1. A passive tracer was used to compute how much of the upper layer fluid was replaced by fluid from the lower layer. In this case, all fluid in layer 1 in the central part of the equatorial region was advected poleward and replaced by upwelling layer 2 fluid. The maximum velocities are larger. In layer 2, the velocities are about twice as large as in case 1, with a maximum of 0.15 m/s. In layer 1, entrainment of layer 2 fluid prevents a doubling of the velocities everywhere in spite a doubling of the forcing. However, the maximum is 1.29 m/s, about twice the maximum found in case 1.

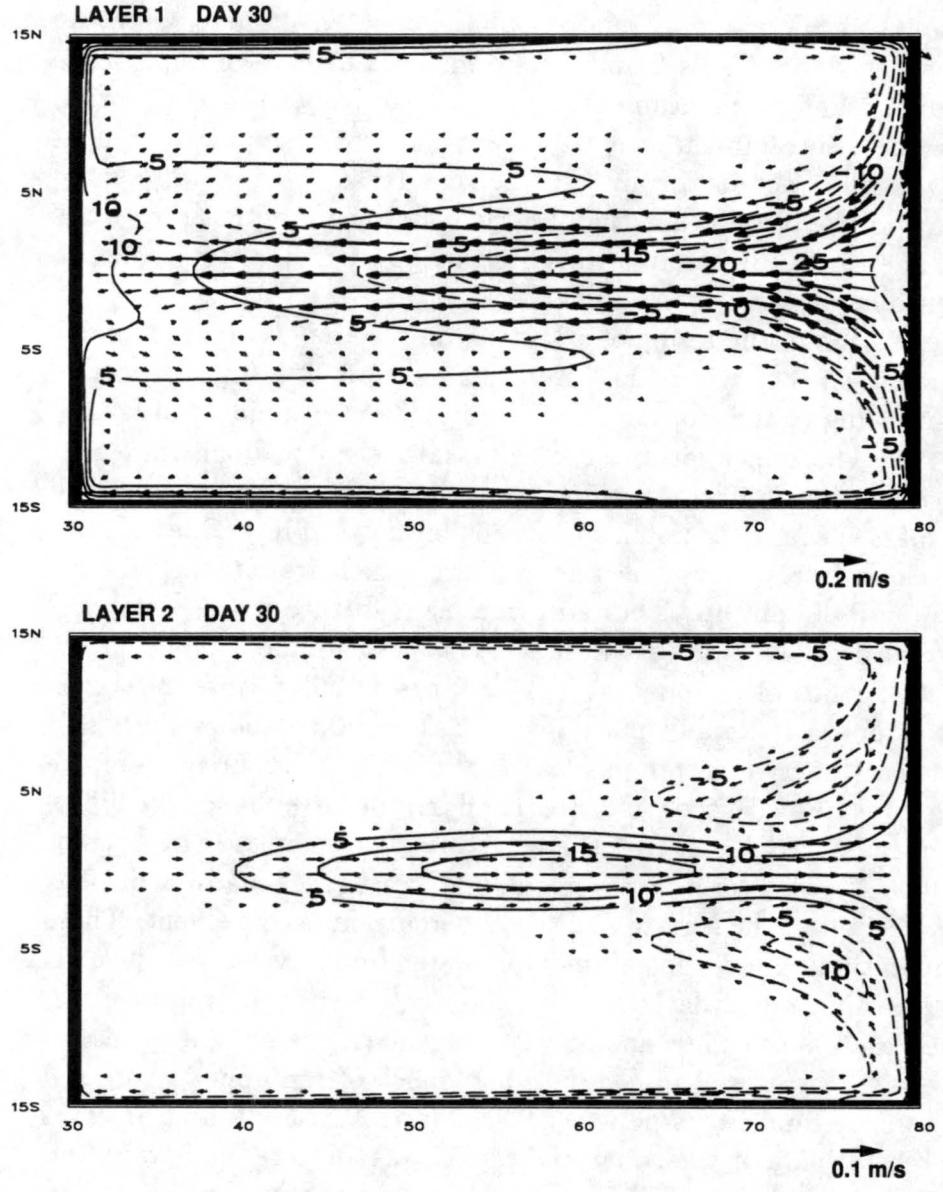

Figure 5.1: Case 1: Linear model without entrainment and detrainment. Layer thickness anomalies (m) and velocities after 30 days. The Yoshida jet is seen in the in upper layer (*top*), and an equatorial undercurrent have been established in layer 2 (*bottom*).

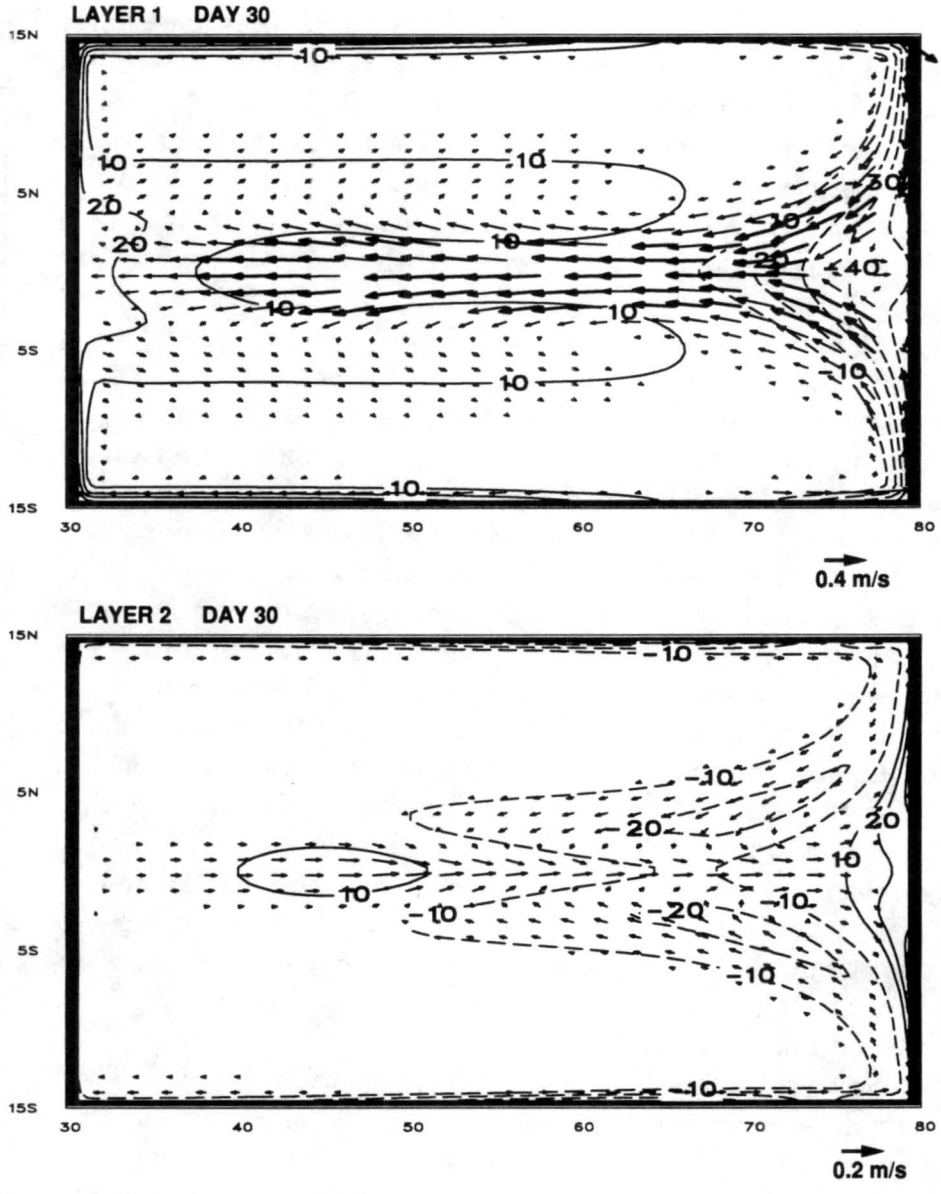

Figure 5.2: Case 2: Linear model with entrainment. Layer thickness anomalies (m) and velocities after 30 days. Equatorial upwelling in upper layer (*top*). An equatorial undercurrent has been established in layer 2 (*bottom*).

Advection of momentum, which is added in case 3, reduces upper layer divergence and thus the entrainment rate. The result is an intensified undercurrent. The maximum current in layer 2 is 0.20 m/s. As seen in Fig. 5.3, the strongest undercurrent is shifted westward of the position it had in the linear case. Apparently, the solution is rather sensitive to the mixing parameterization. However, it should be recalled, that each layer in these three cases represents *different* depth averaged velocities due to the Lagrangian nature of the layers. Due to the reduced entrainment compared to the previous case, only about 65% of the upper layer water is replaced by fluid from the second layer along the equator. Momentum advection acts in this case to reduce the shear in the poleward direction. Consequently, the core of the equatorial jet is wider, and the maximum velocity is somewhat lower, 1.13 m/s.

Active temperature, reduces the vertical stability of the water column in the upwelling region. Case 4 will therefore have a thicker upper layer than case 2 and case 3 (Fig. 5.4). As a result, the maximum velocity in layer 1 is further reduced from the previous cases, to 1.08 m/s. The solution in layer 2 is essentially the same as in case 3. The entrainment of layer 2 fluid is similar to case 3, with about 60% of the fluid displaced along the equator. The reduced stability makes entrainment easier, but the reduced vertical shear compensates for this effect. Otherwise the effect of an active temperature is limited.

Finally, prognostic salinity will further destabilize the water column. In fact layer 1 show now a positive thichness anomaly rather than a negative anomaly due to entrainment of layer 2 fluid. Figure 5.5 shows the result from a run with active entrainment, momentum advection and prognostic temperature and salinity (case 5).

The passive tracer solutions for cases 2-5 are shown in Fig. 5.6. These show the cumulative effects of entrainment during the integration and the amount of upper layer fluid left after 30 days of integration. Only the linear case show coastal upwelling off the equator. The main difference is the for the nonlinear flow, there is divergence near the coast on the equator, while the linear flow is convergent here.

We saw in comparing cases 2 and 3, that momentum advection had a strong impact on the solution. Will this still be the case for the case

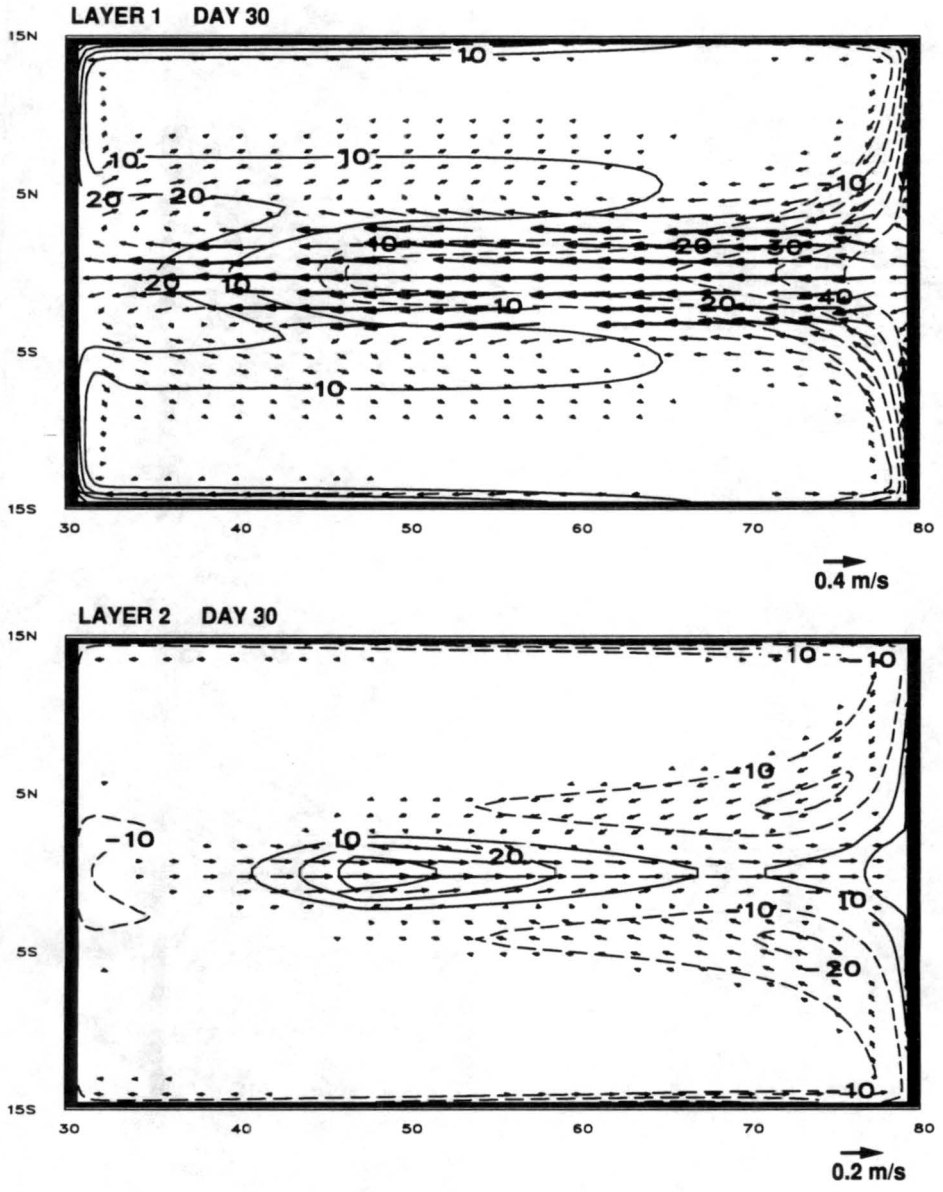

Figure 5.3: Case 3: Nonlinear model with entrainment. Layer thickness anomalies (m) and velocities after 30 days. Upper layer solution (*top*) and layer 2 solution (*bottom*).

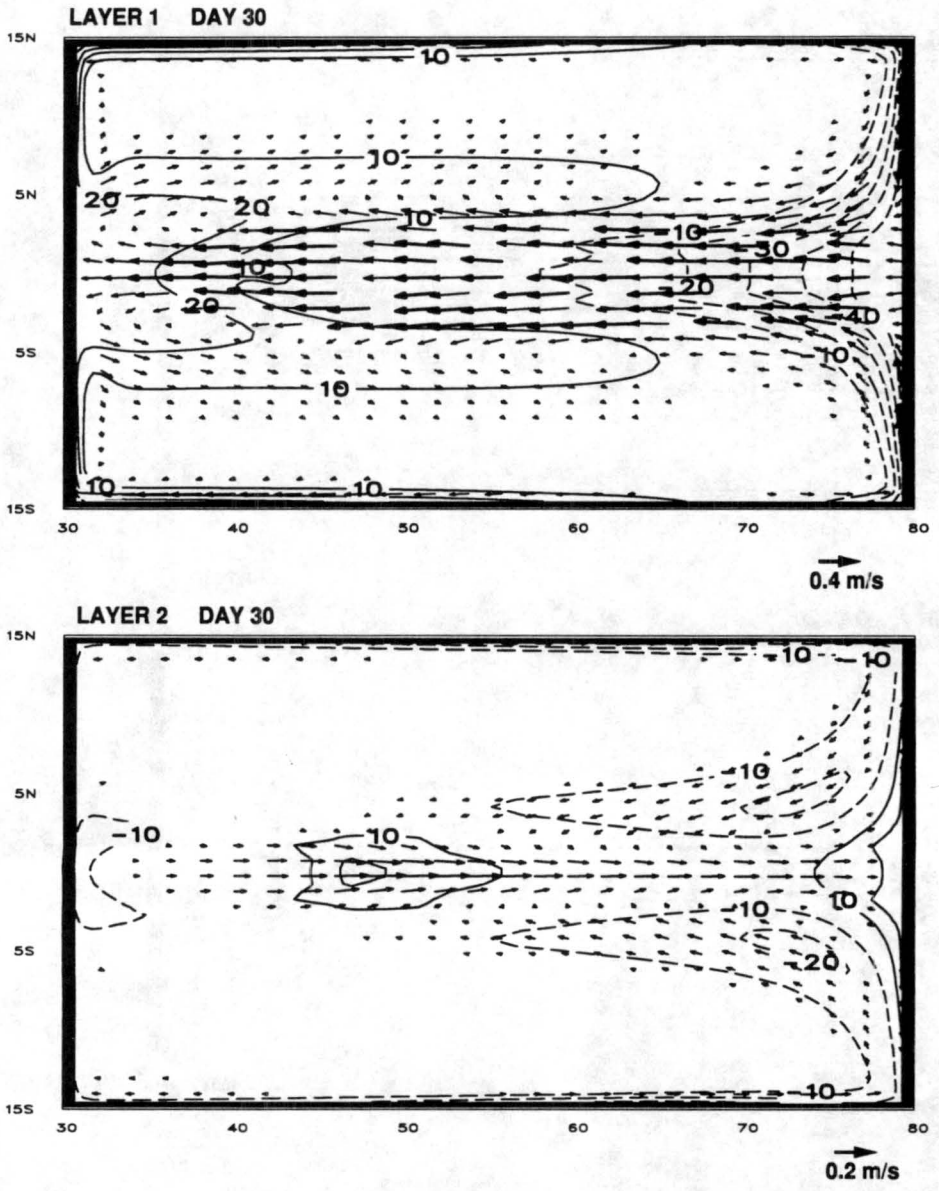

Figure 5.4: Case 4: Nonlinear model with entrainment and prognostic temperature. Layer thickness anomalies (m) and velocities after 30 days. Upper layer solution (*top*) and layer 2 solution (*bottom*).

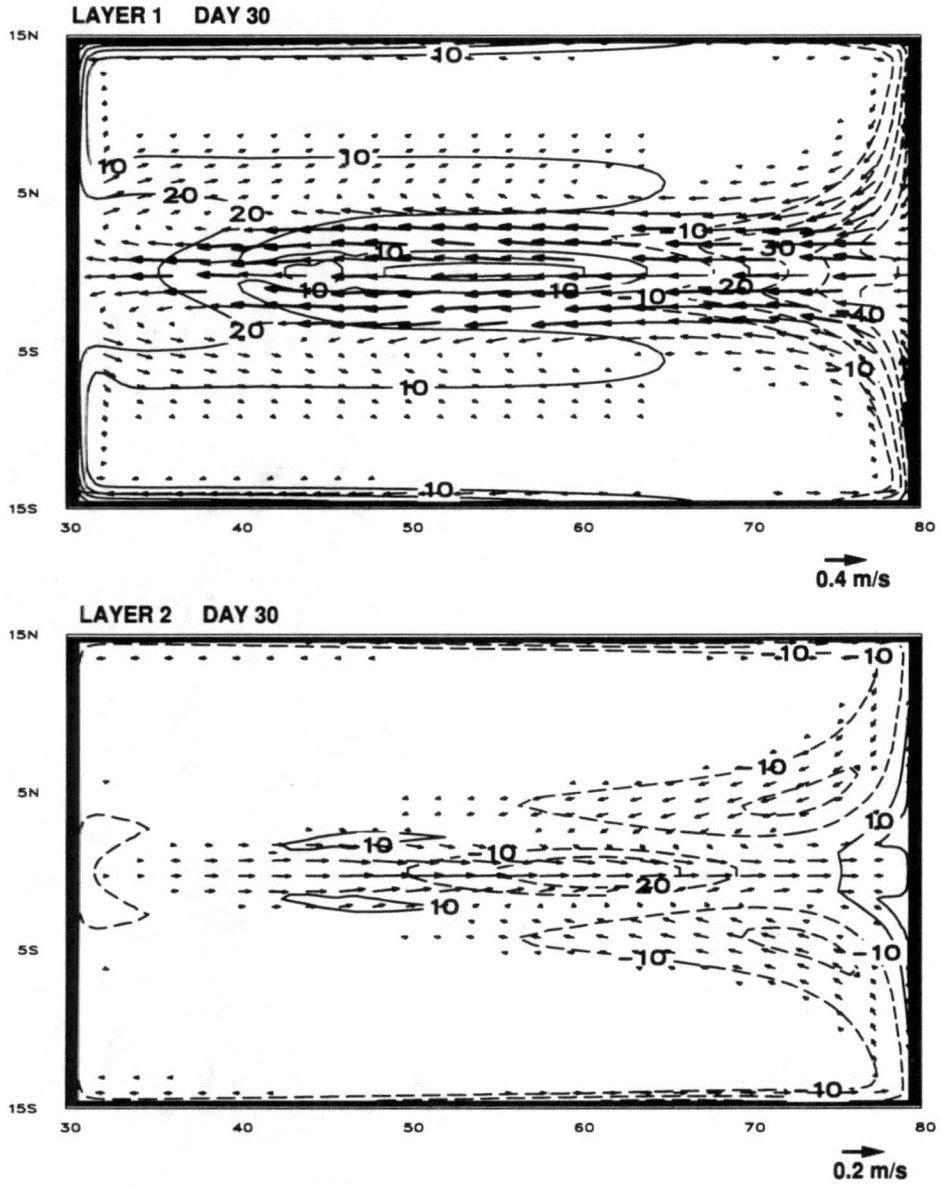

Figure 5.5: Case 5: Layer thickness anomalies (m) and velocities after 30 days. Fully non-linear, thermally active model of equatorial upwelling in upper layer (*top*). An equatorial undercurrent has been established in layer 2 (*bottom*).

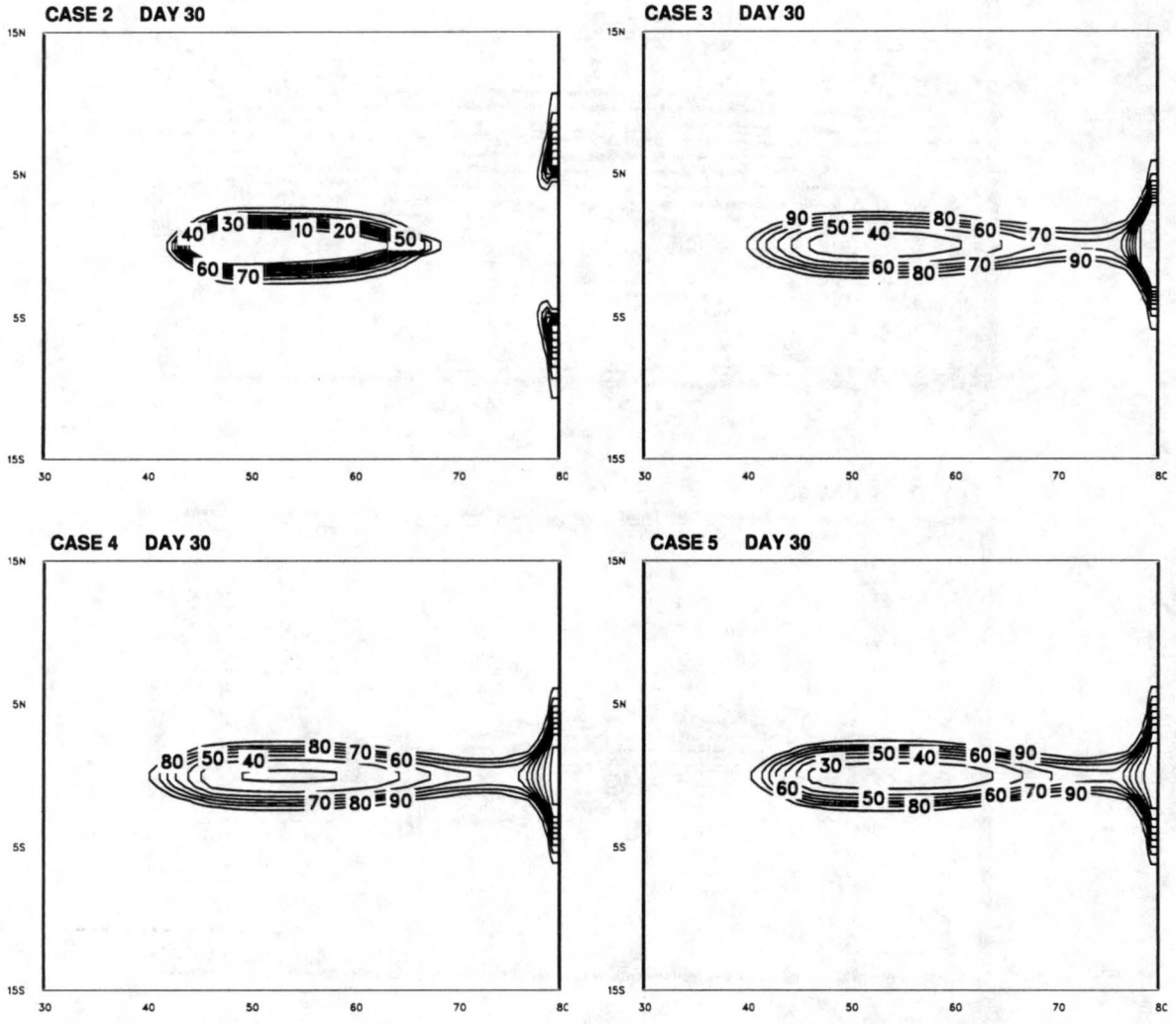

Figure 5.6: Tracer concentrations in layer 1 after 30 days for case 2 (*left, top*), case 3 (*right, top*), case 4 (*left, bottom*) and case 5 (*right, bottom*).

with prognostic temperature and salinity. Case 5 was repeated, but with the non-linear terms in the momentum equation turned off (case 6). The result is shown in Figure 5.7. The solution is similar to that in case 2, but decreased vertical stability results in enhanced equatorial upwelling.

The series of model runs provides the following conclusions: Inertial effects due to momentum advection decreases the equatorial divergence and reduces upwellingsignificantly . They also cause a wider equatorial westward upper layer jet, resulting in stronger eastward flow at poleward latitudes, and before reaching the eastern wall, where there is a stagnation point at the equator, the westward jet splits up in a northward and southward branch. The effects of active temperature on the flow are small. One effect is a steepening of the layer thickness gradient just poleward of the equator, which balance the additional contribution to the pressure gradient by the north-south density gradient.

5.2 Eastward Equatorial Jet

Reversing the wind stress forcing obviously only reverse the linear solution, e.g. depth anomalies ang currents change signs. Along the equator, where the wind is strongest, there is now downwelling, which reduces the influence of non-linear terms. When allowed, detrainment occurs in the east and upwelling occurs in the west along the equator. The effects of the additional physics are small compared to the previous case. Figure 5.7 shows the result of a full physics run at day 35. Note that it is essentially the same solution as one would expect from a linear solution without thermodynamics. The tracer concentrations show the upwelling which takes place in the shear zones just off the equator and along the western wall. Cooling in layer 1 due to entrainment of deep water appears where the concentration is low, while heating occurs in layer 2 in the eastern part of the basin where detrainment is active (not shown). The strenght of a westward undercurrent is sensitive to the parameterization of detrainment. Additional runs, where deepening of the upper layer was much more constrained, results in mass and momentum transfer from layer 1 to layer 2, which will decrease the magnitude or even reverse the undercurrent. How-

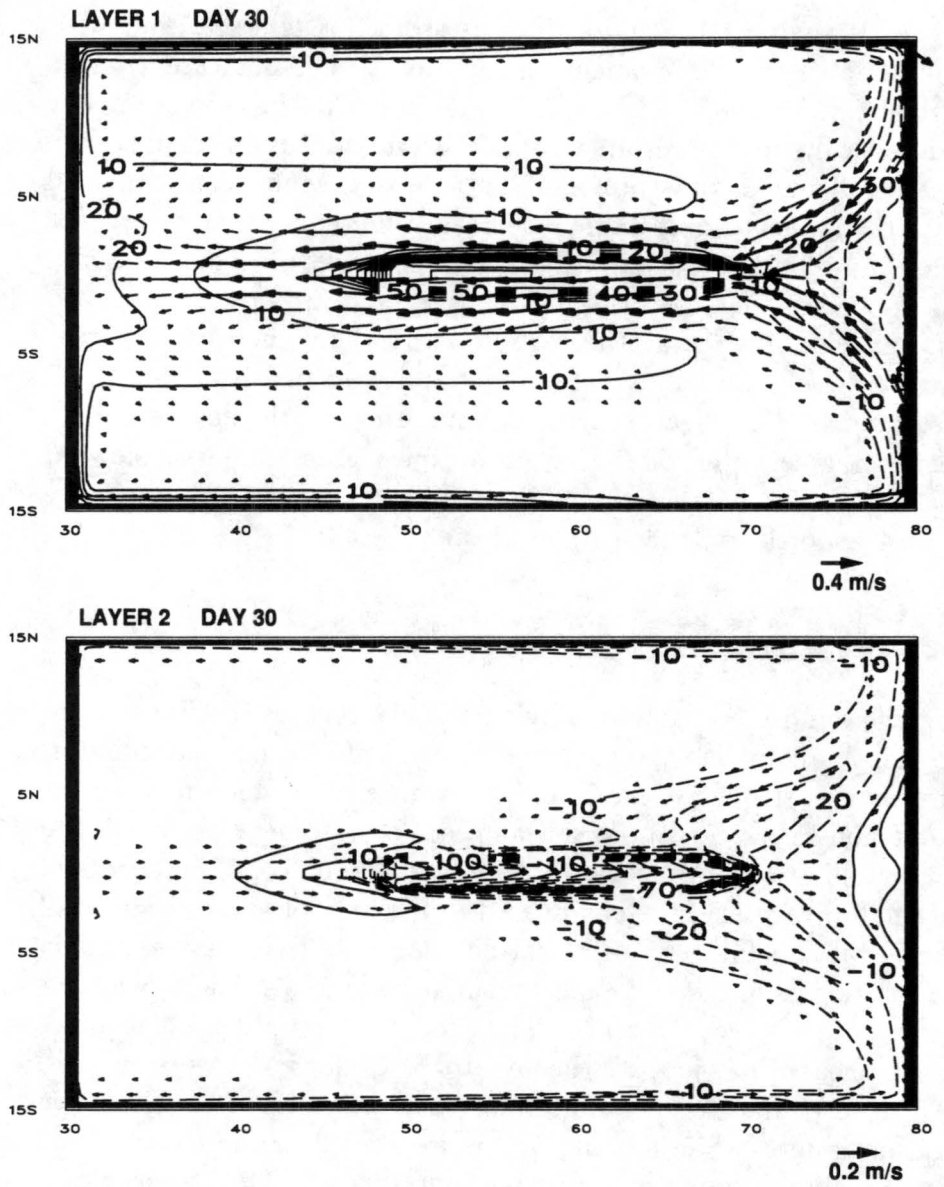

Figure 5.7: Case 6: A linear model with prognostic temperature and salinity with intense equatorial divergence in the upper layer (*top*). Layer 2 has correspondingly intense convergence to supply fluid for entrainment (*bottom*). Layer thickness anomalies (m) and velocities after 30 days.

ever, one should recall that since the average layer thicknesses in a weakly contrained run and strongly constrained will differ considerably, the layers represents different water masses and cannot be directly compared.

5.3 Uniform Steady Wind from the South

This wind field tests coastal upwelling. In the southern hemisphere, upwelling occurs along the eastern edge of the basin, which is the traditionally encoutered coastal upwelling found in such regions as off Peru, California, Oregon, and West Africa. The upwelling in the northern hemisphere is along the western edge of the basin and is similar to the seasonal upwelling found during the Summer Monsoon off Somalia.

The linear case is shown in Figure 5.9. The short term response up to day 30 is dominated by Ekman transport in the interior ocean, that is westward transport in the southern hemisphere and eastward transport in the northern hemisphere. Coastal upwelling is evident along the southeastern boundary and northwestern boundary. Cross equatorial currents exist along the western boundary. The layer thickness anomaly, anti-symmetric around the equator, is that associated with long planetary waves. The propagation of these waves is westward. Upon reflection, the wave length becomes shorter and planetary waves with eastward energy propagation appears. In the real ocean, both short Rossby waves, which have wave lengths less that 2π times the deformation radius, as well as Yanai waves, which may be longer, can carry energy eastward. In the case of anti-symmetric waves which support cross equatorial flow, the longer Yanai waves are most important. The development of the Yanai wave field is seen after day 30. A westward propagating front leaves behind an ocean at rest, but with a parabolic change in layer thickness for both layers. Figure 5.9 show the solution at day 30 and day 180. At day 30 two extrema in the pressure field are found. As time since the onset of the wind pass, an increasing number of extrema occurs. After 60 days there are three major wave crests, after 120 days there are four crests and five at day 180. These extrema are associated with the reflection of westward propagating long Rossby waves into waves with eastward energy propagation, e.g. Yanai

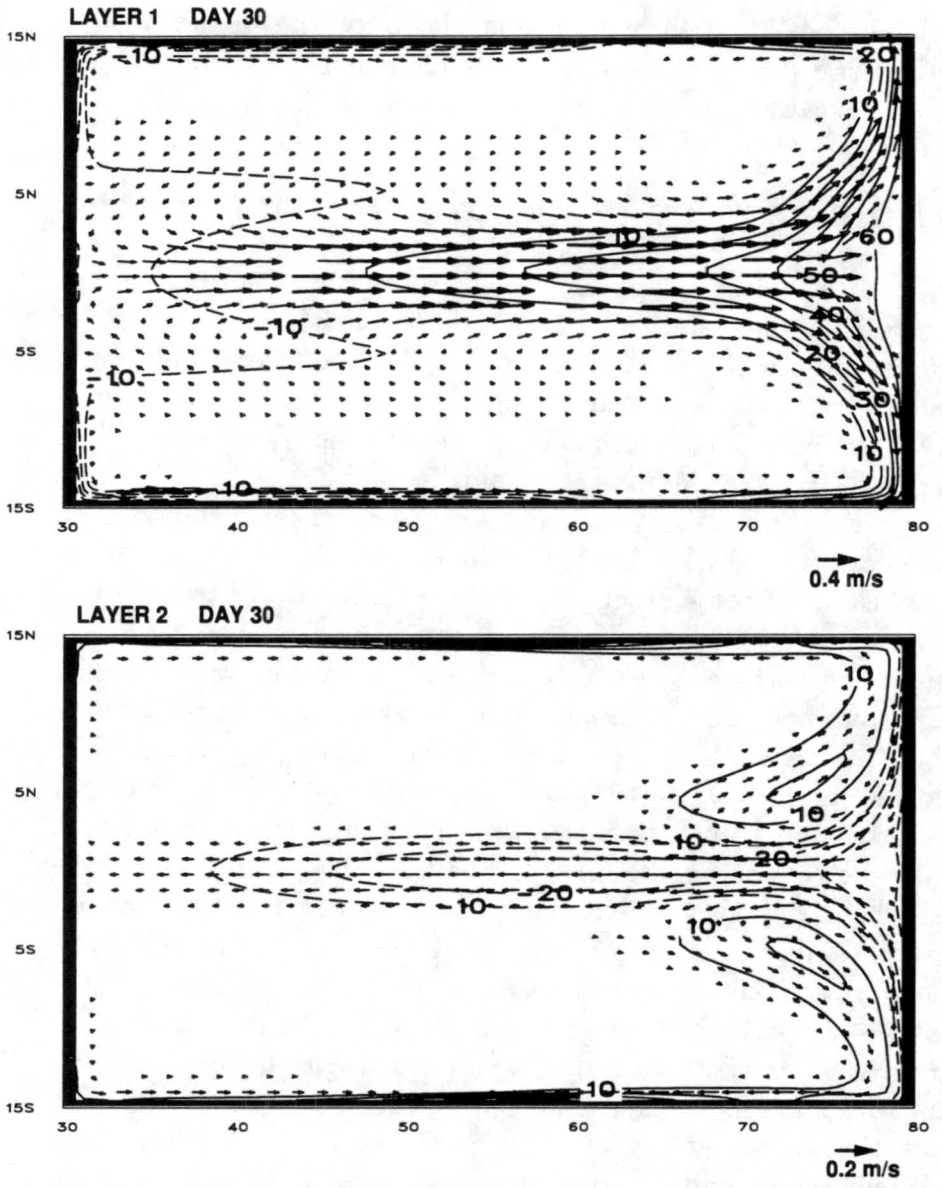

Figure 5.8: Model with prognostic temperature and salinity with intense equatorial convergence in the upper layer (*top*). Layer 2 has a westward jet, driven by high pressure in along the eastern wall (*bottom*). Layer thickness anomalies (m) and velocities after 30 days.

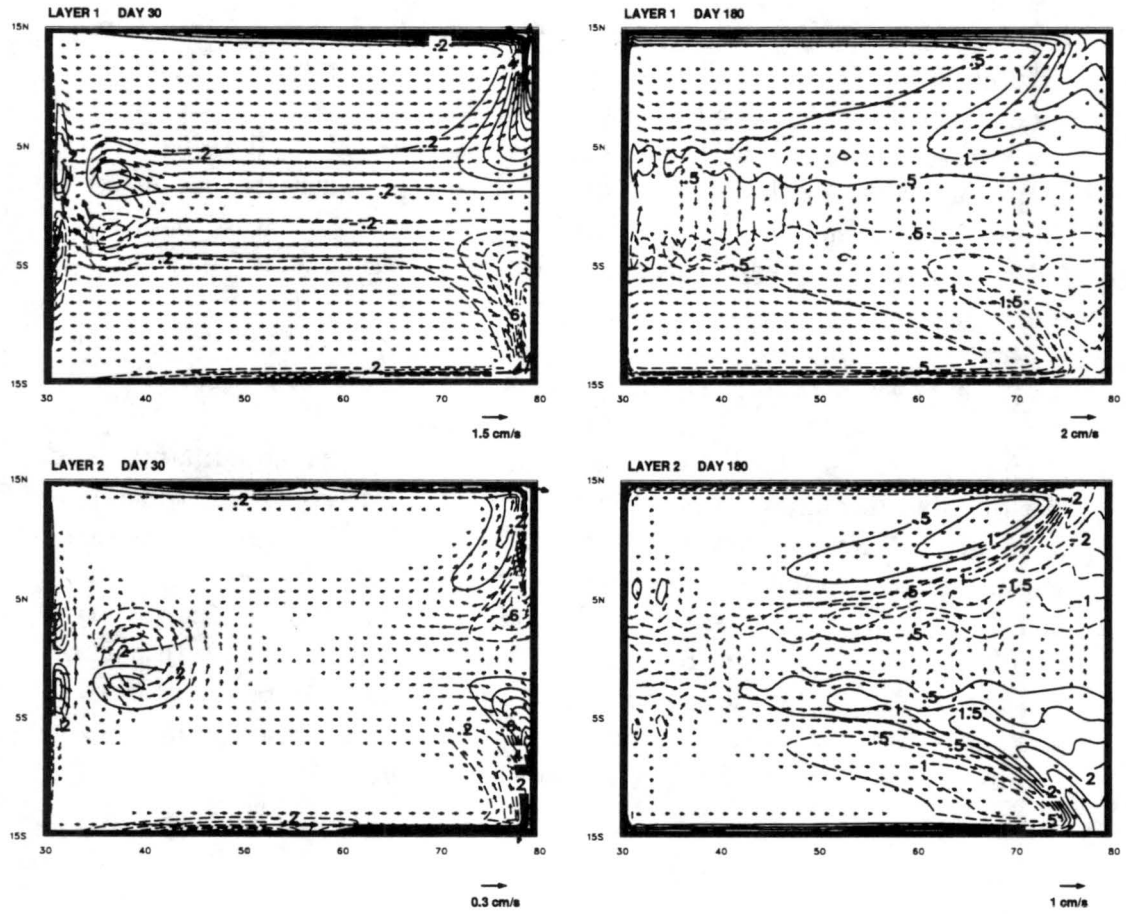

Figure 5.9: Currents and layer thickness anomaly in layer 1 (*top*) and layer 2 (*bottom*) after 30 days (*left*) and after 180 days (*right*) in a linear hydrodynamic model.

waves and short Rossby waves.

For stronger winds a requirement of finite layer thickness may result of material transport between the two active layers. Figure 5.10 shows the currents and thickness from the solution with full physics anomalies and can be compared to the linear case in Fig. 5.9. At day 30, the general circulation pattern is similar to the linear case. However, entrainment of water from layer 2 strongly affects the solution in the southeastern and northwestern parts of the basin. It is also responsible for the asymmetry of the solution along the equator. In the western boundary current north of the equator, strong non-linear eddies form (Fig. 5.10). These are similar to those found in the Indian Ocean in response to the southwest monsoon. At day 30, a strong anti-cyclonic eddy is centered near 5°N, a response similar to the Great Whirl in the Indian Ocean (e.g. Jensen, 1991). Velocities in the strong coastal current are up to 1.5 m/s. After 180 days, short Rossby are radiated away from the northwestern coast.

In the southern hemisphere, a basinwide westward flow maintains a coastal upwelling and results in temperatures as cold as 6°-8°C in the upper layer after 30 days. The eddy generation is less vigorous than in the north western region. Figure 5.11 shows the development of the temperature field in layer 1. The coastal upwelling areas are clearly seen early in the simulation. Cold water is transported offshore in the northwestern part of the basin. This is primarily due to the intense non-linear eddies, which also provides vigorous lateral mixing, limiting the sea surface temperature anomaly. Note that the SST minimum appears offshore.

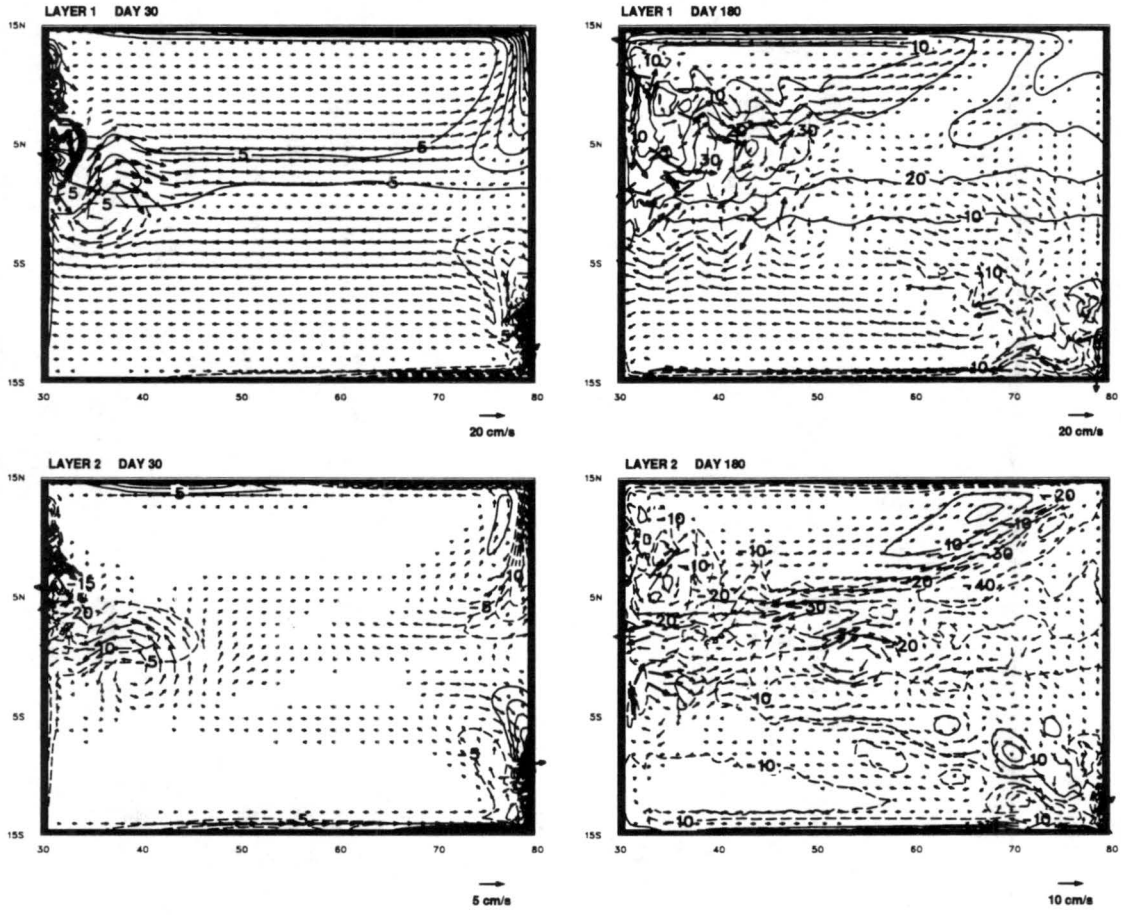

Figure 5.10: Currents and layer thickness anomaly in layer 1 (*top*) and layer 2 (*bottom*) after 30 days (*left*) and after 180 days (*right*) in a non-linear model with active temperature and salinity.

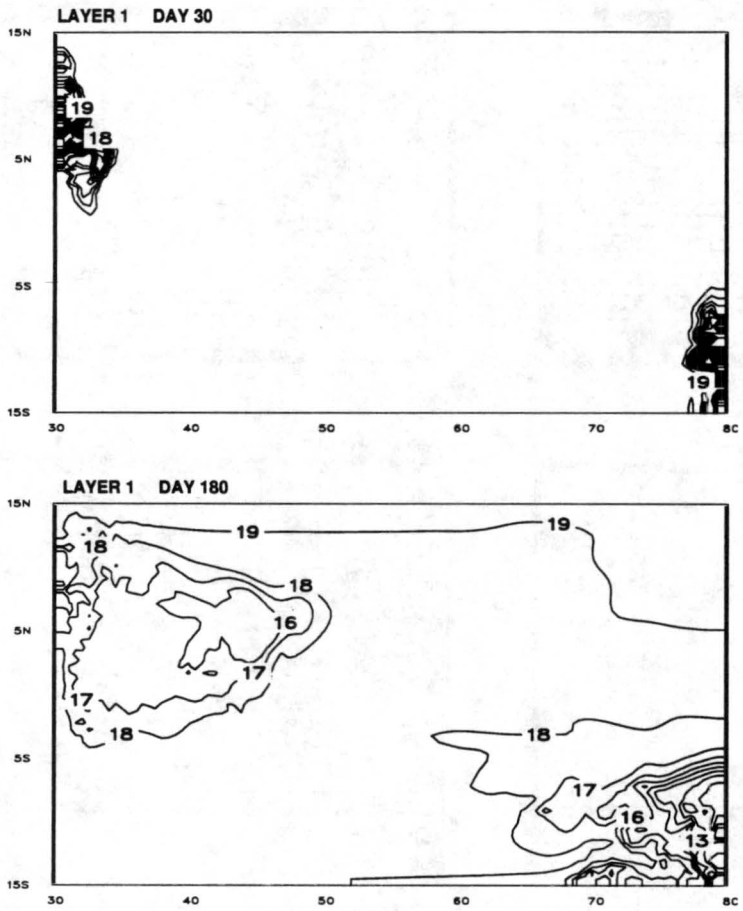

Figure 5.11: Temperature in layer 1 after 30 days (*top*) and after 180 days (*bottom*) in a model with full physics.

Acknowledgements

This research was supported by the CHAMMP program under DOE contract DE-FG03-96ER62167 to Colorado State University. Computer time was provided on the Cray C90 at NERSC, Lawrence Berkeley National Laboratory.

References

Abbott, M. B., McCowan, A. and Warren, I. R., Numerical modelling of free-surface flows that are two-dimensional in plan. In: *Transport Models for Inland and Coastal Waters.* Academic Press, 222–283, 1981.

Arakawa, A. and Y.-J. Hsu, Energy conserving and potential-enstrophy dissipating schemes for the shallow water equations. *Mon. Wea. Rev.*, 118, 1960–1969, 1990.

Arakawa, A. and Lamb, V. R., Computational design of the basic dynamical processes of the UCLA general circulation model. In: *Methods in Computational Physics*, Vol. 17, Academic Press, 174–265, 1977.

Asselin, R., Frequency filter for time integrations. *Mon. Weather Rev.*, 100, 487–490, 1972.

Benson, D. J., Computational methods in Lagrangian and Eulerian hydrocodes, *Comp. Meth. Appl. Mech. Eng.*, 99, 235–394, 1992.

Bleck, R. and D. B. Boudra, Wind-driven spin-up in eddy-resolving ocean models formulated in isopycnic and isobaric coordinates, *J. Geophys. Res.*, 91, 7611–7622, 1986.

Bleck, R., H. P. Hanson, D. Hu and E. B. Kraus, Mixed layer-thermocline interaction in a three-dimensional isopycnic coordinate model. *J. Phys. Oceanogr.*, 19, 1417-1439, 1989.

Bryan, K., A numerical method for the study of the circulation of the world ocean, *J. Comput. Phys.*, 4, 347–376, 1969.

Camerlengo, A. L. and J. J. O'Brien, Open boundary conditions in rotating fluids, J. Comput. Phys., 35, 12–35, 1980.

Gill, A. E., 1982. Atmosphere-Ocean Dynamics. Academic, London, 662 pp.

Hedstrom, G.W., 1979. Nonreflecting boundary conditions for nonlinear hyperbolic systems. J. Comput. Phys., 30: 222–237.

Hirt, C. W., A. A. Amsden , and J. L. Cook, An arbitrary Lagrangian-Eulerian computing method for all flow speeds. *J. Comput. Phys.*, 14, 227-253, 1974.

Hsu, Y.-J. and A. Arakawa, Numerical modeling of the atmosphere with an isentropic vertical coordinate. *Mon. Wea. Rev.*, 118, 1933–1959, 1990.

Hurlburt, H. E., The influence of coastline geometry and bottom topography on the eastern ocean circulation. Ph.D. thesis, The Florida State University, 103 pp, 1974.

Hurlburt, H. E. and J. D. Thompson, A numerical model of the Somali Current, *J. Phys. Oceanogr.*, 6, 646–664, 1976.

James, I. D., A general three-dimensional eddy-resolving model for stratified seas. In: *J. C. J. Nihoul and B. M. Jamart (Eds.): Three-dimensional Models of Marine and Estuarine Dynamics.* Elsevier Oceanogr. Ser., 45, New York, 629 pp., 1987.

Jensen, T. G., A numerical study of the seasonal variability of the Somali Current, Ph.D. dissertation, 118 pp., Florida State Univ., Tallahassee, Feb. 1990.

Jensen, T. G., Modeling the seasonal undercurrents in the Somali current system, *J. Geophys. Res., 96*, 22,151–22,167, 1991.

Jensen, T. G., Equatorial variability and resonance in a wind-driven Indian Ocean model, *J. Geophys. Res., 98*, 22,533–22,552, 1993.

Jensen, T. G., A Quasi-Isopycnal Upper Ocean Model for Climate Modelling. Fifth Symposium on Climate Change Studies, American Meteorological Society, Nashville, 77–80, 1994.

Jensen, T. G., Artificial retardation of barotropic waves in layered ocean models. *Mon. Weather Rev.*, 124, 1272–1283, 1996.

Jensen, T. G., Sensitivity of the tropical Pacific Ocean Circulation to inaccuracies in surface flux forcing. Ninth Conference on Interaction of the Sea and Atmosphere, American Meteorological Society, Phoenix, 87–90, 1998.

Jensen, T. G., Open boundary conditions in stratified ocean models. J. Marine Sys., 16, 297–322, 1998.

Kraus, E. B. and J. S. Turner, A one-dimensional model of the seasonal thermocline, II, The general theory and its consequences. *Tellus*, 119, 98– 106, 1967.

Lighthill, M. J., 1969. Dynamic response of the Indian Ocean to onset of the Southwest Monsoon, Philos. Trans. R. Soc. London, Ser. A, 265: 45–92.

Lilly, D. K., On the computational stability of numerical solutions of the time-dependent non-linear geophysical fluid dynamics problems, *Mon. Weather Rev.*, 93, 11–26, 1965.

Mamayev, O. I. (1975). /it Temperature-Salinity Analysis of World Ocean Waters. Elsevier, New York.

Martinsen, E. A., and H. Engedahl, 1987. Implementation and testing of a lateral boundary scheme as an open boundary condition in a barotropic ocean model. Coastal Eng., 11: 603–627.

McCreary, J. P. and P. K. Kundu, A numerical investigation of the Somali Current during the Southwest Monsoon, *J. Mar. Res.*,46, 25–58, 1988.

McCreary, J. P. and P. K. Kundu, A numerical investigation of sea surface semperature variability in the Arabian Sea, *J. Geophys. Res.*, 94, 16097–16114, 1989.

Oberhuber, J. M., Simulation of the Atlantic Circulation with a coupled sea ice-mixed layer-isopycnal general circulation model. Part I: Model description., *J. Phys. Oceanogr., 23*, 808–829, 1993.

O'Brien, J. J. and H. E. Hurlburt, A numerical model of coastal upwelling, *J. Phys. Oceanogr.*, 2, 14–26, 1972.

Orlanski, I., 1976. A simple boundary condition for unbounded hyperbolic flows. J. Comput. Phys., 21: 251–269.

Pacanowski, R. C. and S. G. H. Philander, Parameterization of vertical mixing in numerical models of the tropical ocean. *J. Phys. Oceanogr., 11*, 1443–1451, 1981.

Røed, L. P. and C. K. Cooper, 1987. A study of various boundary conditions for wind-forced barotropic numerical ocean models. In: J. C. J. Nihoul and B. N. Jamart (Editors), Three-dimensional Models of Marine and Estuarine Dynamics, Elsevier, Amsterdam, pp. 305–335.

Semtner, A. J. and W. R. Holland, Numerical simulation of equatorial ocean circulation. Part I: A basic case in turbulent equilibrium. *J. Phys. Oceanogr. 10*, 667–693, 1980.

Thompson, K. W., 1990. Time-dependent boundary conditions for hyperbolic systems, II. J. Comput. Phys., 89: 436–461.

Yoshida, K., 1959. A theory of the Cromwell Current and equatorial upwelling. *J. Oceanogr. Soc. Jpn.*, **15**, 154–170.

Appendix A

Vertical Normal Modes

In order to apply radiation conditions for each mode separately, we project the solution on vertical normal modes. For simplicity we assume $\partial/\partial y = 0$ in the derivation that follows. We simplify the model equations (2-10) to the linear shallow water equations. In absence of friction, these can be written

$$\frac{\partial U_j}{\partial t} - fV_j = -gH_{oj}\frac{\partial \Phi_j}{\partial x} \tag{A1}$$

$$\frac{\partial V_j}{\partial t} + fU_j = 0 \tag{A2}$$

$$\Phi_j = \gamma \sum_{i=1}^{N}(H_i - H_{oi}) - \sum_{i=1}^{j-1}\frac{(\rho_j - \rho_i)}{\rho_j}(H_i - H_{oi}) \tag{A3}$$

$$\frac{\partial H_j}{\partial t} = -\frac{\partial U_j}{\partial x} \tag{A4}$$

where the notation is the same as in Section 2.

We follow the derivation by Lighthill (1969). Partial differentiation of (A1) with respect to time t and using (A2) gives

$$\frac{\partial^2 U_j}{\partial t^2} + f^2 U_j = -gH_{oj}\frac{\partial^2 \Phi_j}{\partial x \partial t}. \tag{A5}$$

Eliminating H_j using (A3) yields:

$$\left(\frac{\partial^2}{\partial t^2} + f^2\right) U_j = g\,\mathbf{A}\,\frac{\partial^2 \mathbf{U_i}}{\partial \mathbf{x^2}}, \tag{A6}$$

where the $N \times N$ matrix $\mathbf{A}$ has the elements given by

$$\mathrm{a_{ji}} = \left(\gamma - \frac{\rho_\mathrm{j} - \rho_\mathrm{min(j,i)}}{\rho_\mathrm{j}}\right)\mathrm{H_{oj}}. \tag{A7}$$

Plane wave solutions of the form $U_j = \mathcal{U}_j \exp(-i(\kappa x - \omega t))$ must satisfy the relation

$$(\omega^2 - f^2)\mathcal{U}_j = g\kappa^2\,\mathrm{a_{ji}}\,\mathcal{U}_\mathrm{i}, \tag{A8}$$

where ω is the angular frequency, κ is the wavenumber, and $\mathcal{U}_j$ is an amplitude.

We can expand on vertical normal modes by writing

$$U_j = \sum_{k=1}^{N} \alpha_{jk}\tilde{U}_k \tag{A9}$$

where α_{jk} is component j of eigenvector k of the matrix $\mathbf{A}$. The normal mode amplitudes are computed from

$$\tilde{U}_k = (\alpha_{jk})^{-1} U_j, \tag{A10}$$

where $(\alpha_{jk})^{-1}$ denotes the inverse of matrix α_{jk}. For free waves, the dispersion relation is from (A8) and (A10)

$$\omega^2 - f^2 - gh^{(n)}k^2 = 0 \tag{A11}$$

where $h^{(n)}$ is the equivalent depth, i.e. an eigenvalue to $\mathbf{A}$.

Along an open boundary, we compute the amplitude of the normal modes from the transport in each layer using (A10) and apply the OBC to each mode. The amplitudes for each mode on the boundary are then transformed back using (A9). This calculation involves two matrix multiplications and is fairly fast. However, note that the calculation of these matrices requires finding eigenvalues and eigenvectors as well as inverting an $N \times N$ matrix. For this reason we use a time and space independent reference state, so it is only done once. In cases where the stratification changes with space and time, the normal mode matrices should in principle be recalculated during the integration.

Appendix B

Derivation of Characteristic Open Boundary Conditions

Below we will illustrate how the method of characteristics (e.g. Thompson, 1990) can be applied to an open boundary condition. We will use the linear shallow water equations on an f-plane:

$$\frac{\partial U}{\partial t} - fV = -gH_o\frac{\partial \eta}{\partial x} \tag{B1}$$

$$\frac{\partial V}{\partial t} + fU = -gH_o\frac{\partial \eta}{\partial y} \tag{B2}$$

$$\frac{\partial \eta}{\partial t} = -\frac{\partial U}{\partial x} - \frac{\partial V}{\partial y} \tag{B3}$$

where the notation is given in section 2. We can write equations (B1)-(B3) in matrix form:

$$\begin{pmatrix} U \\ V \\ \eta \end{pmatrix}_t + \underline{\mathbf{A}} \begin{pmatrix} U \\ V \\ \eta \end{pmatrix}_x + \underline{\mathbf{B}} \begin{pmatrix} U \\ V \\ \eta \end{pmatrix}_y + \underline{\mathbf{C}} = 0 \tag{B4}$$

where the subscript denotes differentiation and the coefficient matrices $\underline{\mathbf{A}}$, $\underline{\mathbf{B}}$ and $\underline{\mathbf{C}}$ are given by

$$\underline{\mathbf{A}} = \begin{bmatrix} 0 & 0 & c^2 \\ 0 & 0 & 0 \\ 1 & 0 & 0 \end{bmatrix} \tag{B5}$$

$$\underline{\mathbf{B}} = \begin{bmatrix} 0 & 0 & 0 \\ 0 & 0 & c^2 \\ 0 & 1 & 0 \end{bmatrix} \tag{B6}$$

$$\underline{\mathbf{C}} = \begin{pmatrix} -fV - F \\ fU - G \\ 0 \end{pmatrix} \tag{B7}$$

Each direction will be considered separately. For the x-direction, we have:

$$\begin{pmatrix} U \\ \eta \end{pmatrix}_t + \underline{\mathbf{A}}' \begin{pmatrix} U \\ \eta \end{pmatrix}_x + \underline{\mathbf{C}}' = 0 \tag{B8}$$

where

$$\underline{\mathbf{A}}' = \begin{bmatrix} 0 & c^2 \\ 1 & 0 \end{bmatrix} \tag{B9}$$

and

$$\underline{\mathbf{C}}' = \begin{pmatrix} -fV - F \\ \partial V/\partial y \end{pmatrix} \tag{B10}$$

The eigenvalues for A' are $\pm c$. We will select a pair of eigenvectors

$$\begin{pmatrix} -c \\ 1 \end{pmatrix} \quad \text{and} \quad \begin{pmatrix} c \\ 1 \end{pmatrix} \tag{B11}$$

and define a matrix $\underline{\mathbf{S}}$ which consists of these eigenvectors and its inverse:

$$\underline{\mathbf{S}} = \begin{bmatrix} c & -c \\ 1 & 1 \end{bmatrix} \quad \text{and} \quad \underline{\mathbf{S}}^{-1} = \begin{bmatrix} \frac{1}{(2c)} & \frac{1}{2} \\ -\frac{1}{(2c)} & \frac{1}{2} \end{bmatrix} \tag{B12}$$

It is easily seen that we can diagonalize $\underline{\mathbf{A}}$ using these matrices:

$$\underline{\mathbf{S}}^{-1}\,\underline{\mathbf{A}}\,\underline{\mathbf{S}} = \begin{bmatrix} c & 0 \\ 0 & -c \end{bmatrix} = \underline{\mathbf{\Lambda}} \tag{B13}$$

If we apply $\underline{\mathbf{S}}^{-1}$ to Eqn. (B8) we get

$$\begin{bmatrix} \frac{1}{(2c)} & \frac{1}{2} \\ -\frac{1}{(2c)} & -\frac{1}{2} \end{bmatrix} \begin{pmatrix} U \\ \eta \end{pmatrix}_t + \underline{\mathcal{L}} + \underline{\mathbf{S}}^{-1} \underline{\mathbf{C}}' = 0 \qquad (B14)$$

where the characteristic vector, $\underline{\mathcal{L}}$, is defined as in Thompson (1990), i.e.

$$\mathcal{L} = \begin{pmatrix} \mathcal{L}_1 \\ \mathcal{L}_2 \end{pmatrix} = \begin{bmatrix} \frac{1}{2} & \frac{C}{2} \\ \frac{1}{2} & -\frac{C}{2} \end{bmatrix} \begin{pmatrix} U \\ \eta \end{pmatrix}_x = \begin{pmatrix} \frac{1}{2}(U + c\eta)_x \\ \frac{1}{2}(U - c\eta)_x \end{pmatrix} \qquad (B15)$$

After finding the characteristic (B15), we now transform (A14) back by applying $\underline{\mathbf{S}}$. We can write

$$U_t + c(\mathcal{L}_1 - \mathcal{L}_2) - fV - F = 0 \qquad (B16)$$

$$\eta_t + (\mathcal{L}_1 + \mathcal{L}_2) + V_y = 0 \qquad (B17)$$

At a right boundary, an outgoing wave propagates with the velocity $+c$ and an incoming (i. e. reflected) wave propagates with the velocity $-c$. We do not want a reflected wave, so we set

$$\mathcal{L}_2 = \frac{1}{2}(U - c\eta)_x = 0 \qquad (B18)$$

on boundary. Using this in (B16) and (B17), we have on the right boundary:

$$\frac{\partial \tilde{U}}{\partial t} = -\frac{1}{2} c^{(k)} \frac{\partial}{\partial x}(\tilde{U} + c^{(k)}\tilde{\eta}) + f\tilde{V} + \tilde{F} \qquad (B19)$$

$$\frac{\partial \tilde{\eta}}{\partial t} = -\frac{1}{2}\frac{\partial}{\partial x}(\tilde{U} + c^{(k)}\tilde{\eta}) - \frac{\partial \tilde{V}}{\partial y} \qquad (B20)$$

where $\tilde{\Phi}$ indicates that the amplitude of the vertical mode k of a variable Φ rather than the amplitude for each layer should be used in the stratified case. For a left boundary we get equations similar to (B19) and (B20).